ADVANCED ENGINEERING MATERIALS



DOI: 10.1002/adem.200900094

# In Situ Observation of Dynamic Recrystallization in the Bulk of Zirconium Alloy**

By *Klaus-Dieter Liss*, Ulf Garbe, Huijun Li, Thomas Schambron, Jonathan D. Almer* and *Kun Yan*

Dynamic recrystallization broadly occurs in thermo-mechanical processes, examples of which include metal forming,[1] the formation of the Earth's crust,[2,3] and the flow of glaciers.[4] This process impacts a correspondingly broad range of areas including the mechanical properties of industrial products,[5] the size limitation of nano-crystalline materials,[6] the occurrence of earthquakes,[7] and the simulation of polar ice sheets in climatic change.[8] Dynamic recrystallization results from a competition between thermally driven nucleation and growth processes, as well as grain breakage and refinement during plastic deformation. Although this phenomenon is well understood in a general sense, predictions for a specific system are enormously difficult due to dependence on a number of variables including chemical composition, temperature, strain, strain rate, and thermo-mechanical history. Here, we present unprecedented in situ observations of dynamic recrystallization in individual bulk crystallites of a macroscopic Zircaloy-4 specimen under thermo-mechanical load. The microstructural kinetics, grain statistics, and crystallographic correlations inherent to this process are revealed. Utilizing synchrotron high-energy X-ray diffraction[9] allows direct observation of dynamic recrystallization and related effects in real time and at high temperature. Conventionally, such effects were either studied retrospectively after quenching, during which additional phase transitions may occur, or indirectly through changes in physical properties, relying on empirical experience or on the surface only using electron microscopy. Even more potential of this work may be raised by future material scientists, engineers, and industry on tailoring their metal products by thermo-mechanical simulation directly in a synchrotron beam.

In classical powder X-ray diffraction, individual crystallites of the sample are ideally randomly oriented and their number is high, in order to find statistically enough crystallites to diffract radiation into any direction of observation, under the condition that Bragg's law is fulfilled. This ideal condition leads to Debye–Scherrer cones which are projected into concentric rings when scattered onto a two-dimensional detector oriented perpendicular to the primary beam. The condition of isotropy is no longer fulfilled if the illuminated volume of the sample is small compared to its grain size, leading to individual illuminated spots on the Debye–Scherrer rings as seen in Figure 1. These reflections stem from a small number of crystallites, which ought to be oriented on the Ewald sphere, in order to reflect to the observed positions. The number of distribution of reflections, their orientation, and their correlations give insight into grain size, texture, and orientation relationships of the crystallites. This has been elaborated earlier[10] and will be employed in the present study.

High-energy X-rays (as used here at 90 keV) have small diffraction angles and therefore scatter in the forward direction, allowing collection of full Debye–Scherrer rings in transmission geometry.[9] With only small photo absorption, they probe the whole thickness of the sample revealing information from grains fully embedded in the bulk. The nuclear reactor structural material Zircaloy-4 grade R60804 of nominal composition (in wt%) Zr, 1.5% Sn, 0.2% Fe, 0.1% Cr, 0.1% O is used for the present study. It crystallizes in a hexagonal closed packed (hcp) $\alpha$-Zr structure below 1083 K and a body centered cubic (bcc) $\beta$-Zr structure above 1253 K.[11] The 5-mm-thick specimens were put into a servo-hydraulic load frame with the load axis perpendicular to the incoming X-ray beam of $0.2 \times 0.2\,mm^2$ size. The sample was heat treated in air with zero load in order to allow recovery and growth of distinguishable grain sizes by ramping the temperature up to 1277 K and subsequent cooling. Diffraction patterns were then recorded upon application of a constant load of 225 N corresponding to an

[*] *Dr. K.-D. Liss, Dr. U. Garbe, Dr. H. Li, K. Yan*
*Australian Nuclear Science and Technology Organisation, BMP 1 Menai NSW 2234 (Australia)*
*E-mail: kdl@ansto.gov.au; liss@kdliss.de*
*T. Schambron, K. Yan*
*Faculty of Engineering, University of Wollongong Wollongong, NSW 2522 (Australia)*
*Dr. J. D. Almer*
*Advanced Photon Source, Argonne National Laboratory Argonne, IL 60439 (USA)*

[**] *This work was supported by the Australian Synchrotron Research Program, which is funded by the Commonwealth of Australia under the National Collaborative Research Infrastructure Strategy. The experimentalists especially thank the XOR beamline members and the APS user office for support. Use of the APS was supported by the U.S. Department of Energy under contract DE-AC02-06CH11357.*

   

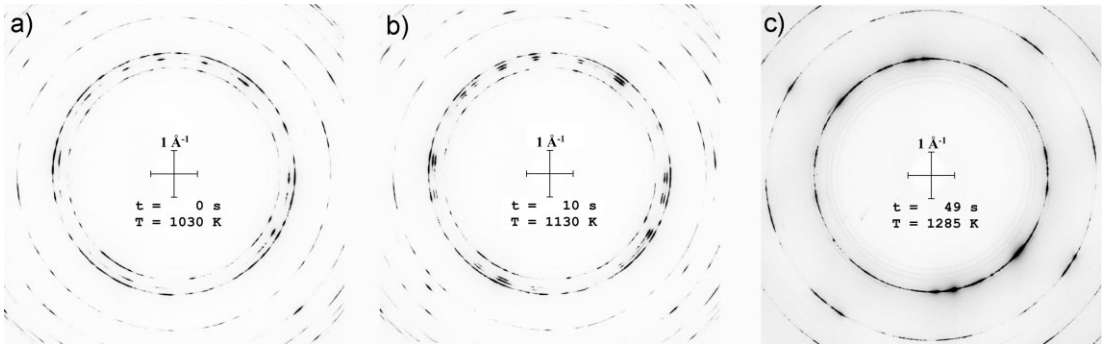


*Fig. 1. Debye–Scherrer rings of different stages of the heating cycle with time t and temperature T: (a) in the α-Zr phase, (b) α + β – Zr two-phase field, and (c) in the β-Zr phase. The cross denotes the center of the rings and defines the scale of 1 Å$^{-1}$.*

initial stress of 7.5 MPa, while the temperature was increased from 688 to 1283 K in 60 s. The diffraction patterns were taken continuously with a 0.2 s frame rate for 60 s. Images showing various stages of the process are displayed in Figure 1. Azimuthal integration of the Debye–Scherrer rings leads to conventional powder diffraction patterns, which are depicted in Figure 2 evolving in time. Only peaks from the low-temperature α-phase appear in Figure 1(a) and at time $t = 0$ of Figure 2. The morphology of the rings suggests that the grains are fairly large, as compared to the illuminated volume, with an estimate of a few 100 μm.[10] Furthermore, the spots show a mosaic spread of 2° indicating a sub-grain structure with small-angle grain boundaries. They are attributed to a Widmanstätten-like microstructure, as it occurs in Zr[12] and homologous Ti,[13] which is created during the phase transformation upon cooling in the previous heat treatment. At $t_1 = 7$ s the high-temperature β-phase appears (Fig. 1(b)) in coexistence with the α-phase which vanishes completely after $t_2 = 24$ s (Fig. 1(c)). The reflections on the appearing β-110 ring lie well aligned with those of α-002, proving the transformation fulfills the Burgers orientation relation to a high degree.[14,15] In order to represent the time evolution of the reflections, a selected ring is cut at the bottom position in Figure 1, radially integrated over the entire peak and straightened clockwise 0–360° into a horizontal line of Figure 3, the second dimension being time. The above-mentioned orientation correlation is recognized by comparing the angular positions of the timelines of reflections from the two phases.

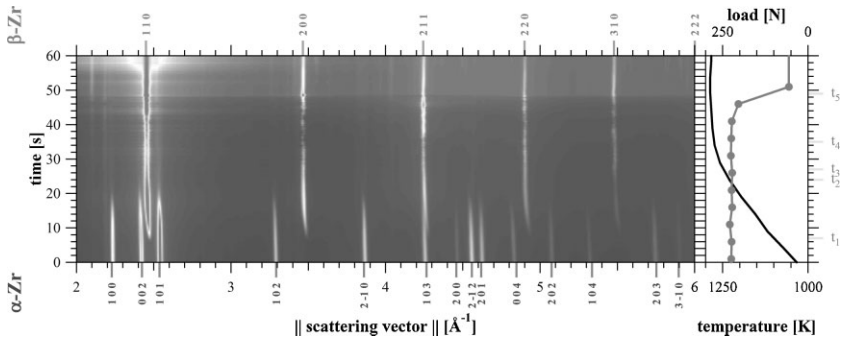


*Fig. 2. Color-coded powder diffraction lines evolving in time upon heating.*

Depending on how they are counted (intensity and splitting), there are about 20 reflections on the α-Zr 002 Debye–Scherrer ring, which transform into β-Zr 110, with a very similar pattern as expected from their Burgers relation. The β-Zr 200 and β-Zr 211 rings, respectively, show about half and double the numbers of spots as compared to β-Zr 110, which is understood by the ratio of the multiplicity of the three reflections being 6, 24, and 12, respectively. Since the grains are randomly oriented, this distribution is fulfilled statistically, but for non-overlapping reflections one can say their number is proportional to the number of reflecting grains in the illuminated volume, or inversely proportional to the grain size. Moreover, the number of observed spots is proportional to the solid angle each reflection occupies, expressed by its mosaic spread. A reflection with a larger mosaic spread is more likely to intersect the Ewald sphere than that of a perfect crystal.

These figures show that there is grain coarsening in the β-phase at roughly $t_2 = 24$ s, after the α-phase has fully disappeared. Thermal activation is high and there is no second phase left to restrain grain growth, while the yield strength of the material in this temperature range is still high enough to prevent rapid plastic deformation. With increasing temperature starting after $t_3 = 27$ s, timelines of reflections from the individual crystallites become spotty. Here the grains are split into sub-grains. In a cold deformation process, continuous broadening of the grains' mosaic spread, which evolves into the final texture state, would be expected. In contrast, we observe the appearance and disappearance of reflection spots which can be attributed to a dynamic recovery process. This is the first time the process has been observed in situ. Highly distorted sub-grains recover to form a smaller number of more perfect sub-grains, which then break up again upon further deformation, repeating the process, and leading to a globally steady state. Eventually, small-angle boundaries between distinct sub-grains accumulate and split into individual timelines and a larger overall mosaic distribution, as seen at the 20°, 40°, and 80° grains in β-Zr 110 and β-Zr 220 in Figure 3. In addition, grain rotation of a few degrees is observed, expressed by a curved

  

ADVANCED ENGINEERING MATERIALS



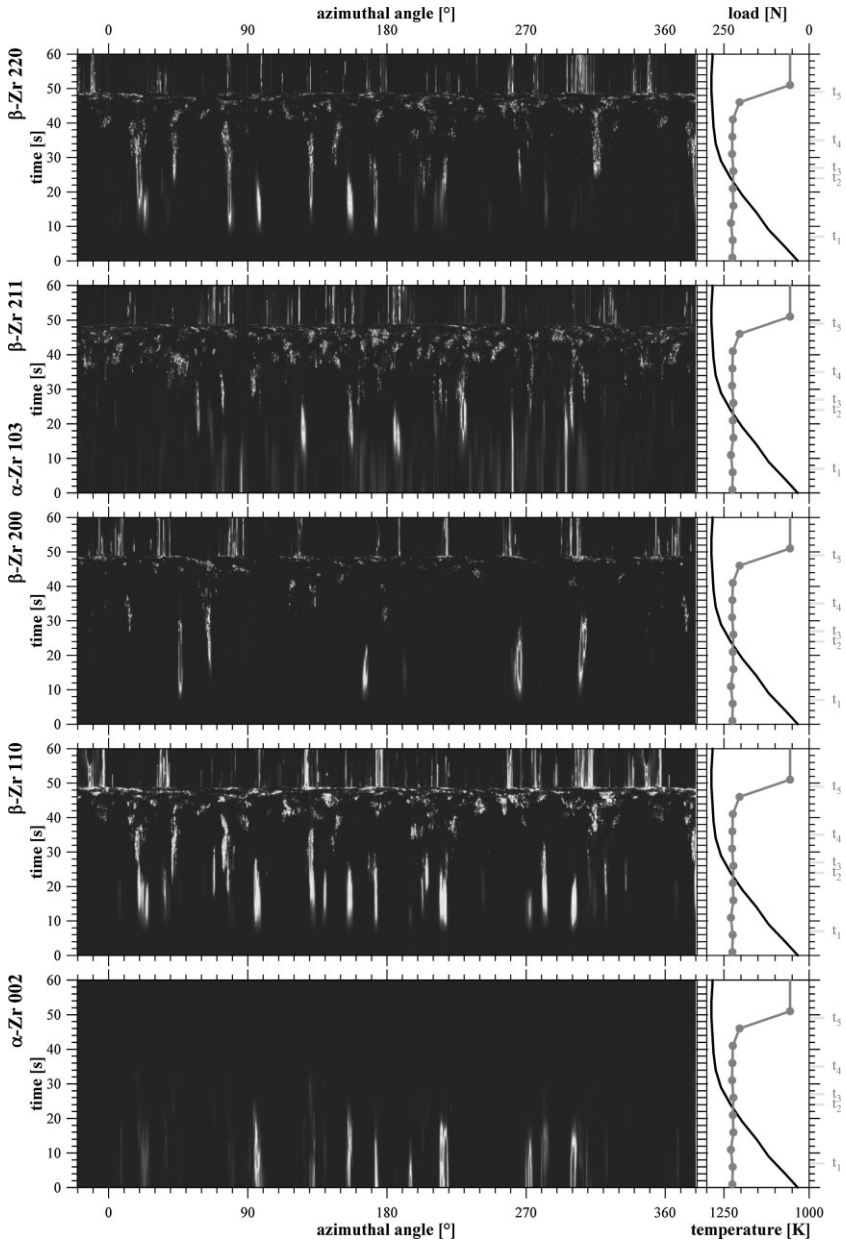


*Fig. 3. Time evolution of the color-coded intensity distribution on selected Debye–Scherrer rings as a function of azimuthal angle. The line and line-symbol diagrams to the right denote the temperature and load parameters, respectively. Time events $t_1$–$t_5$ are referred to in the text.*

or inclined timeline such as seen at 80° and 155° azimuthal angles of β-Zr 220 and many others. It should be noted that upon recovery, highly perfect, virtually dislocated free sub-grains are created for a short time showing low mosaic spread and, thus, are found less probable to fulfill the Ewald condition, which describes the observed decrease in intensity in the timeline of the grain.

The regime of dynamic recrystallization is entered upon further increase in temperature, strain, and strain rate (as necking occurs) and it is characterized by the sudden appearance and fluctuation of new orientations[16] starting slowly after $t_4 = 35$ s and escalating until rupture of the specimen at $t_5 = 49$ s, after which the load drops to zero and static recovery and grain growth takes place, indicated by straight, coarsening timelines. Some of the new grains are temporal islands in orientation space, particularly well seen in the β-Zr 110 and β-Zr 211 maps of Figure 3, extending azimuthally up to 10° and with a well-expressed sub-grain orientation structure. Others evolve in string-of-pearl-like timelines appearing as caustics, one of which is well expressed at 70° in β-Zr 200. Here, the dynamic recovery/recrystallization process leads to a little stepwise but large grain rotation of an almost perfect crystallite extending over 40° and accelerating with increasing temperature. Similarly, the previously stated time-orientation islands rotate through dynamic recovery of their sub-grain groups, but then making larger 10° jumps on similar caustics driven to recrystallization by a larger angular offset.

One of the fingerprints of dynamic recrystallization at low strain rates is the oscillatory behavior of the stress–strain curve when recrystallization is completed faster than the deformation. It is expressed in the stepwise evolution of the caustics and the spottiness of the timelines, revealing that almost perfect crystal volumes are created for a short time which then need to overcome their activation energy in order to break up due to plastic deformation. Interestingly, these fluctuations occur on both the sub- and inter-grain scales, suggesting that dynamic recovery and dynamic recrystallization have much in common, although they are distinct in nature.

In conclusion, we have followed the typical thermo-mechanical response of a metal in situ and rapidly in real time on the example of a zirconium alloy. Statistics and orientation correlations of embedded/bulk material grains were deduced from two-dimensional X-ray diffraction patterns. Upon heating little grain growth occurs in the low-temperature α-Zr phase which then transforms gradually into β-Zr. Plastic deformation accelerates at higher temperatures and regimes of dynamic recovery and dynamic recrystallization could clearly be distinguished.

*Received: March 19, 2009*
*Final Version: April 6, 2009*

  

[1] Y. V. R. K. Prasad, T. Seshacharyulu, *Int. Mater. Rev.* **1998**, *43*, 243.
[2] D. L. Kohlstedt, B. Evans, S. J. Mackwell, *J. Geophys. Res.* **1995**, *100*, 17587.
[3] H. W. Green, H. Jung, *Elements* **2005**, *1*, 31.
[4] S. J. Marshall, *Earth Planet. Sci. Lett.* **2005**, *240*, 191.
[5] P. D. Hodgson, R. K. Gibbs, *ISIJ Int.* **1992**, *32*, 1329.
[6] S. C. Tjong, H. Chen, *Mater. Sci. Eng. R* **2004**, *45*, 1.
[7] L. G. J. Montesi, G. Hirth, *Earth Planet. Sci. Lett.* **2003**, *211*, 97.
[8] G. E. Flowers, S. J. Marshall, H. Bjornsson, G. K. C. Clarke, *J. Geophys. Res.* **2005**, *110*, F02011 1.
[9] K.-D. Liss, A. Bartels, A. Schreyer, H. Clemens, *Textures Microstruct.* **2003**, *35*, 219.
[10] K.-D. Liss, A. Bartels, H. Clemens, S. Bystrzanowski, A. Stark, T. Buslaps, F.-P. Schimansky, R. Gerling, C. Scheu, A. Schreyer, *Acta Mater.* **2006**, *54*, 3721.
[11] Y.-E. Kim, J.-W. Park, J. Cleveland, *IAEA* **2006**; IAEA-TECDOC-1496.
[12] M. K. Kumar, I. Samajdar, N. Venkatramani, G. K. Dey, R. Tewari, D. Srivastava, S. Banerjee, *Acta Mater.* **2003**, *51*, 625.
[13] D. Phelan, M. Reid, N. Stanford, R. Dippenaar, *JOM-US* **2006**, *58*, 67.
[14] W. G. Burgers, *Physica* **1934**, *1*, 561.
[15] A. J. J. Van Ginneken, W. G. Burgers, *Acta Crystallogr.* **1952**, *5*, 548.
[16] C. Chauvy, P. Barberis, F. Montheillet, *Mater. Sci. Forum* **2004**, *467-470*, 1151.



  